

Memory Efficient Mutual Information-Maximizing Quantized Min-Sum Decoding for Rate-Compatible LDPC Codes

(Extended Version)

Peng Kang, Kui Cai, Xuan He, and Jinhong Yuan

Abstract—In this letter, we propose a two-stage design method to construct memory efficient mutual information-maximizing quantized min-sum (MIM-QMS) decoder for rate-compatible low-density parity-check (LDPC) codes. We first develop a modified density evolution to design a unique set of lookup tables (LUTs) that can be used for rate-compatible LDPC codes. The constructed LUTs are optimized based on their discrepancy values and a merge function to reduce the memory requirement. Numerical results show that the proposed rate-compatible MIM-QMS decoder can reduce the memory requirement for decoding by up to 94.92% compared to the benchmark rate-compatible LUT-based decoder with generally faster convergence speed. In addition, the proposed decoder can approach the performance of the floating-pointing belief propagation decoder within 0.15 dB.

Index Terms—Low-density parity-check (LDPC) codes, lookup table (LUT), mutual information-maximizing (MIM), rate-compatible.

I. INTRODUCTION

Low-density parity-check (LDPC) codes [1] have been widely applied to many practical applications, such as wireless communication and data storage systems [2]–[4], for their powerful error correction capability under iterative message passing decoding [5]. Many decoding algorithms have been developed for the LDPC codes to achieve a good trade-off between the performance and decoding complexity [6], [7].

Recently, lookup table (LUT)-based decoders [8]–[14] drew considerable attention due to their simple table lookup operations and excellent error performance with coarse quantization. Specifically, the LUT-based decoder in [8] is designed based on the density evolution (DE) [5], which aims at minimizing the asymptotic error probability. As an alternative, the LUT-based decoders in [9]–[14] focus on maximizing the mutual information between the coded bits and the extrinsic messages. In [9]–[11], several sets of LUTs need to be constructed respectively to update the nodes with different degrees at each iteration. This causes a large memory requirement for storing the LUTs when the node degree or the decoding iteration becomes large. To reduce the memory usage, the mutual-information-maximizing quantized min-sum (MIM-QMS) decoder was proposed in [14], which utilizes the integer additions and one set of LUTs to update all nodes with different degrees.

On the other hand, many practical communication and data storage systems prefer to adopt the rate-compatible codes instead of the fixed-rate codes, e.g., [3], [4], [15]. This is because the rate-compatible LDPC codes can improve the system reliability more efficiently by adapting different code rates according to the channel conditions [3]. However, most of the LUT-based decoders e.g., [10] and [14], are designed for an LDPC code with a particular code rate, which is not capable of supporting rate-compatibility. Although the rate-compatible LUT-based decoder in [11] is able to reuse the LUTs

of several LDPC codes across different code rates, it suffers from performance loss, which increases with the number of reused LUTs due to the mismatch problem. Moreover, there are a large number of intermediate LUTs required for the decoding process in [9]–[11], which vary with both node degrees and iterations. Obviously, this increases the memory requirement for hardware implementation.

In this letter, we aim at designing a memory efficient MIM-QMS decoder for the rate-compatible LDPC codes. To this end, we propose a two-stage design method for the construction of the LUTs. In particular, we modify the MIM-DE presented in [14] by considering the joint degree distributions of all target LDPC codes rather than their individual degree distributions. Compared to the LUTs designed in [10] and [14], this allows us to construct a unique set of iteration-varying LUTs used for various code rates. We further propose a metric, named as the discrepancy value, and a merge function to optimize the constructed LUTs with similar entries. Instead of minimizing the degradation of asymptotic performance for reducing the memory variation as in [10], our proposed LUT optimization method focuses on maximizing the mutual information between the coded bit and the extrinsic messages. We demonstrate that the proposed MIM-QMS decoder can save the memory requirement by up to 94.92% compared to the rate-compatible LUT-based decoder [11] with faster convergence speed in the moderate-to-high signal-to-noise (SNR) region. Moreover, it shows only minor performance degradation compared to the MIM-QMS decoders designed for fixed-rate codes, and also approaches the performance of the floating-pointing belief propagation (BP) decoder.

II. PRELIMINARIES

A. Notations

In this letter, calligraphy capitals are used to define an alphabet set. Normal capitals denote the random variables. Lower-case letters denote the realization of a random variable. Boldface letters are used to define a vector.

B. The MIM-QMS decoder

Consider a (q_m, q_v) MIM-QMS decoder [14], where q_m is the precision of the exchanged messages between check nodes (CNs) and variable nodes (VNs), and q_v is the precision of a posteriori probability (APP) messages. Note that we set $q_v > q_m$ to avoid clipping because the APP messages are generally larger than the exchanged messages. During the decoding iterations, the MIM-QMS decoder processes the messages belonging to certain alphabet sets. Define $\mathcal{L} = \{0, 1, \dots, |\mathcal{L}| - 1\}$ as the alphabet set of the channel output, where $|\cdot|$ is the

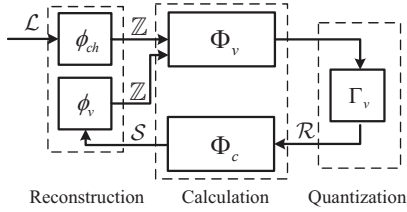


Fig. 1: The framework of the MIM-QMS decoder.

cardinality of the set. Denote the alphabets of variable-to-check (V2C) and check-to-variable (C2V) messages by $\mathcal{R} = \{0, 1, \dots, |\mathcal{R}| - 1\}$ and $\mathcal{S} = \{0, 1, \dots, |\mathcal{S}| - 1\}$, respectively. In this letter, we consider $|\mathcal{R}| = |\mathcal{S}| = |\mathcal{L}| = 2^{q_m}$. As depicted in Fig. 1, the MIM-QMS decoder performs reconstruction, calculation, and quantization steps for decoding, which can be described correspondingly by three types of functions:

1) *Reconstruction*: The reconstruction function maps a q_m -bit message to a specific number in the integer domain \mathbb{Z} . We denote the reconstruction functions of the channel output and the C2V message by ϕ_{ch} and ϕ_v , respectively.

2) *Calculation*: The computing function for the CN update takes the q_m -bit V2C messages as the input, and outputs the q_m -bit C2V messages based on the cluster MS algorithm [10]. For the VN update, the computing function takes the q_m -bit channel output with all other q_m -bit reconstructed C2V messages to calculate the V2C messages with q_v -bit precision.

3) *Quantization*: The quantization function quantizes a q_v -bit V2C message into a q_m -bit message based on a threshold set denoting by Γ_v . Here the threshold set is determined by the dynamic programming [16] aiming to maximize the mutual information between the coded bit and the V2C message.

Given a discretized binary-input additive white Gaussian noise channel (AWGNC) with the noise standard deviation σ_d and the degree distributions of an LDPC code with a specific code rate, the MIM density evolution (MIM-DE) is used in [14] to construct the LUTs associated to the reconstruction functions and the threshold set by tracking the evolution of the probability mass functions (pmfs) at each iteration. Note that σ_d is known as the design noise standard deviation, which is carefully selected to maximize the mutual information between the coded bit and the V2C message for a preset maximum decoding iteration.

III. DESIGN OF MEMORY EFFICIENT MIM-QMS DECODERS FOR RATE-COMPATIBLE LDPC CODES

In [9], [10], [12] and [14], the LUT-based decoders and the MIM-QMS decoders are designed for an LDPC code with a fixed code rate. We refer to these decoders as the rate-specific decoders. When different LDPC codes are adopted by the system, these rate-specific decoders such as [10] and [14] need to store multiple sets of LUTs corresponding to different LDPC codes for decoding. This increases the memory demand for hardware implementation. In this section, we propose a two-stage design method to construct a unique set of LUTs for the MIM-QMS decoder, which can be used for decoding rate-compatible LDPC codes with significantly reduced memory requirement.

A. Stage 1: LUT Design Based on the Modified MIM-DE

In [14], the MIM-QMS decoders are designed by using the MIM-DE based on the degree distributions of one target LDPC code. To construct the MIM-QMS decoder for rate-compatible LDPC codes, we first propose a modified MIM-DE, which

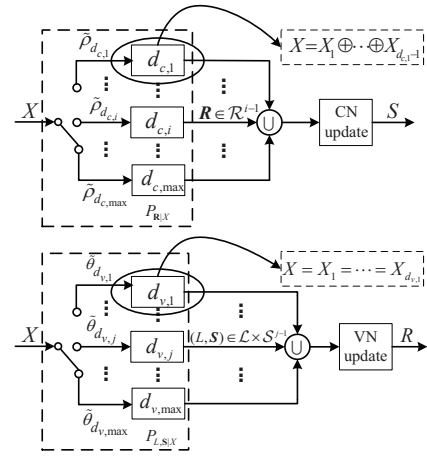


Fig. 2: The framework of the MIM-QMS decoder for decoding the rate-compatible LDPC codes.

considers the degree distributions of all target LDPC codes simultaneously. Denoting the sets of the CN and VN degrees of K target LDPC codes by $\tilde{\mathcal{D}}_c$ and $\tilde{\mathcal{D}}_v$, we have

$$\begin{aligned} \tilde{\mathcal{D}}_c &= \bigcup_{k=1}^K \mathcal{D}_{c,k} = \{d_{c,1}, d_{c,2}, \dots, d_{c,\max}\}, \\ \tilde{\mathcal{D}}_v &= \bigcup_{k=1}^K \mathcal{D}_{v,k} = \{d_{v,1}, d_{v,2}, \dots, d_{v,\max}\} \end{aligned} \quad (1)$$

where $\mathcal{D}_{c,k}$ and $\mathcal{D}_{v,k}$ refer to the sets of the CN and VN degrees of the k -th LDPC code, respectively. Define the joint degree distributions as

$$\tilde{\rho}(\zeta) = \sum_{i \in \tilde{\mathcal{D}}_c} \tilde{\rho}_i \zeta^{i-1}, \quad \tilde{\theta}(\zeta) = \sum_{j \in \tilde{\mathcal{D}}_v} \tilde{\theta}_j \zeta^{j-1}, \quad (2)$$

where $\tilde{\rho}_i$ and $\tilde{\theta}_j$ are the fractions of edges incident to the CNs with degree- i and the VNs with degree- j , respectively, by considering the Tanner graphs [17] of all target LDPC codes. We denote the random variable for the coded bit by X , which takes values from $\mathcal{X} = \{0, 1\}$. Denote the random variable for the channel output by L , and the random variable for the V2C (resp. C2V) message by R (resp. S). Define $P_{L|X}$ as the pmf of channel output L conditioned on the coded bit X . Define $P_{R|X}$ and $P_{S|X}$ as the pmfs of the V2C message R and the C2V message S conditioned on the coded bit X , respectively.

As illustrated by Fig. 2, for the CN update, the V2C messages are classified into $|\tilde{\mathcal{D}}_c|$ alphabet sets correspondingly to different CN degrees. The modified MIM-DE aims to compute the conditional pmf $P_{S|X}$ based on the joint CN degree distribution. Denote the vector of V2C messages sent to a degree- i ($i \in \tilde{\mathcal{D}}_c$) CN by $\mathbf{R} \in \mathcal{R}^{i-1}$. Define $\mathbf{r} = (r_1, r_2, \dots, r_{i-1}) \in \mathcal{R}^{i-1}$ as a realization of \mathbf{R} . According to the independent and identical distribution (i.i.d) assumption [5], the joint pmf $P_{\mathbf{R}|X}$ at a degree- i CN is given by

$$P_{\mathbf{R}|X}(\mathbf{r}|x) = \left(\frac{1}{2}\right)^{i-2} \sum_{\mathbf{x}: \oplus \mathbf{x} = x} \prod_{k=1}^{i-1} P_{R|X}(r_k|x_k), \quad (3)$$

where $x \in \mathcal{X}$ is a realization of X , and $\mathbf{x} = (x_1, x_2, \dots, x_{i-1})$ is the vector of coded bits associated to the neighboring VNs. Here $\oplus \mathbf{x} = x$ means the checksum of the CN is satisfied. Denote a realization of the C2V message $S \in \mathcal{S}$ by s . For each incoming realization \mathbf{r} , the computing function Φ_c calculates the corresponding output s by performing the MS operation [10]. Considering all possible values $s \in \mathcal{S}$ for each CN alphabet set and the fraction $\tilde{\rho}_i$ in (2), the V2C messages in

each CN alphabet set contribute to the output C2V messages with probability $\tilde{\rho}_i$. Therefore, we obtain

$$P_{S|X}(s|x) = \sum_{i \in \tilde{\mathcal{D}}_c} \tilde{\rho}_i \cdot \sum_{\substack{\mathbf{r} \in \mathcal{R}^{i-1}, \\ \Phi_c(\mathbf{r})=s}} P_{\mathbf{R}|X}(\mathbf{r}|x), \quad (4)$$

where Φ_c is given by [14, Eq. (16)]

$$\Phi_c(\mathbf{r}) = f^{-1} \left(\prod_{k=1}^{i-1} \text{sgn}(f(r_k)) \cdot \min_{k=1,2,\dots,i-1} (|f(r_k)|) \right). \quad (5)$$

Here $f(\cdot)$ maps the V2C messages in $\mathcal{R} = \{0, 1, \dots, 2^{q_m} - 1\}$ correspondingly to an integer set $\{2^{q_m-1}, \dots, 1, -1, \dots, -2^{q_m-1}\}$, and $f^{-1}(\cdot)$ operates as the inverse function of $f(\cdot)$.

For the VN update, as shown by Fig. 2, the C2V messages are characterized by $|\tilde{\mathcal{D}}_v|$ alphabet sets corresponding to different VN degrees. The modified MIM-DE calculates the conditional pmf $P_{R|X}$ based on the joint VN degree distribution. Denote the vector of the C2V messages and the channel output at a degree- j ($j \in \tilde{\mathcal{D}}_v$) VN by $(L, \mathbf{S}) \in \mathcal{L} \times \mathcal{S}^{j-1}$. Define $\mathbf{s} = (s_1, s_2, \dots, s_{j-1}) \in \mathcal{S}^{j-1}$ as a realization of \mathcal{S}^{j-1} . The joint pmf $P_{L, \mathbf{S}|X}$ at a degree- j VN can be computed by

$$P_{L, \mathbf{S}|X}(l, \mathbf{s}|x) = P_{L|X}(l|x) \prod_{k=1}^{j-1} P_{S|X}(s_k|x). \quad (6)$$

Define \mathcal{B} as the alphabet set of the q_v -bit V2C message calculated by the computing function for the VN update, where $B \in \mathcal{B}$ is the random variable for the q_v -bit V2C message. Let $P_{B|X}$ be the pmf of B conditioned on the coded bit X . According to the fraction $\tilde{\theta}_j$ in (2), the C2V messages (L, \mathbf{S}) in each VN alphabet set contribute to the output V2C messages with probability $\tilde{\theta}_j$ so that we have

$$P_{B|X}(b|x) = \sum_{j \in \tilde{\mathcal{D}}_v} \tilde{\theta}_j \cdot \sum_{\substack{(l, \mathbf{s}) \in \mathcal{L} \times \mathcal{S}^{j-1}, \\ \Phi_v(l, \mathbf{s})=b}} P_{L, \mathbf{S}|X}(l, \mathbf{s}|x) \quad (7)$$

for a realization b of B . Note that the computing function Φ_v is given by [14, Eq. (4)]

$$\Phi_v(l, \mathbf{s}) = \phi_{ch}(l) + \sum_{k=1}^{j-1} \phi_v(s_k). \quad (8)$$

By taking \mathcal{B} and $P_{B|X}$ as inputs, we perform the dynamic programming (DP) [16] to obtain the threshold set Γ_v for the VN update, and the conditional pmf of the V2C message $P_{R|X}$. We refer $\mathbf{DP}(\cdot)$ to the DP operation, which can be described as

$$[P_{R|X}, \Gamma_v] = \mathbf{DP}(\mathcal{B}, P_{B|X}). \quad (9)$$

In addition, the threshold set for bit decision, denoted by Γ_e with $|\Gamma_e| = 1$, also needs to be designed for each iteration, which is obtained similarly to Γ_v by considering $(l, \mathbf{s}) \in \mathcal{L} \times \mathcal{S}^j$.

B. Stage 2: LUT Optimization

In general, the LUT constructed by the modified MIM-DE is assumed to result in distinct LUTs for different iterations, i.e., the reconstruction functions and the threshold sets vary with iterations. Apparently, storing these iteration-varying LUTs increases the memory requirement. We notice that the LUTs corresponding to the same reconstruction function or threshold set has similar entries for certain consecutive iterations. This is because the pmfs computed by the modified MIM-DE hardly change during these iterations. A similar phenomenon is also observed in [5] for the conventional DE. Motivated by this observation, we propose an LUT optimization method in this section, which reuses one optimized LUT for different consecutive iterations to reduce the memory requirement.

Algorithm 1 LUT Optimization Process

Input: Q^* , I_{\max} , $\mathbf{y}^{(t)}$ for $t = 1, 2, \dots, I_{\max}$
Output: Optimized LUTs $\mathbf{y}^{*(t)}$ for $t = 1, 2, \dots, I_{\max}$

- 1: $\Delta d^* = 0$, $k = 1$
- 2: **while** $k \leq I_{\max} - 1$ **do**
- 3: Compute $\Delta d^{(k)} = d(\mathbf{y}^{(k)}, \mathbf{y}^{(k+1)})$ by (10)
- 4: **if** $\Delta d^{(k)} \leq \Delta d^*$ **then**
- 5: $k = k + 1$, go to step 3
- 6: **else**
- 7: Set $M = 1$, $\mathcal{I}_1 = \{1\}$
- 8: **for** $t = 1 : I_{\max} - 1$ **do**
- 9: **if** $d(\mathbf{y}^{(t)}, \mathbf{y}^{(t+1)}) \leq \Delta d^{(k)}$ **then**
- 10: $\mathcal{I}_M = \mathcal{I}_M \cup \{t + 1\}$
- 11: **else**
- 12: $M = M + 1$, $\mathcal{I}_M = \{t + 1\}$
- 13: **end if**
- 14: **end for**
- 15: Update $\tilde{\mathbf{y}}^{(m)} = f(\{\mathbf{y}^{(t)} : t \in \mathcal{I}_m\})$ based on (11) for $m = 1, 2, \dots, M$
- 16: Run the modified MIM-DE with $\tilde{\mathbf{y}}^{(m)}$, $m = 1, 2, \dots, M$
- 17: Compute the mutual information $Q^{(k)}$ at I_{\max}
- 18: **if** $Q^{(k)} \geq Q^*$ and $\Delta d^{(k)} \geq \Delta d^*$ **then**
- 19: $\Delta d^* = \Delta d^{(k)}$
- 20: $\mathbf{y}^{*(t)} = \tilde{\mathbf{y}}^{(m)}$, $\forall t \in \mathcal{I}_m$
- 21: **end if**
- 22: $k = k + 1$
- 23: **end if**
- 24: **end while**

Consider an LUT for either the reconstruction function or the threshold set at the t -th iteration, which can be represented by a vector $\mathbf{y}^{(t)} = (y_1^{(t)}, y_2^{(t)}, \dots, y_N^{(t)})$. Here N is the total number of entries in the LUT, which is determined by the bit precision q_m . More specifically, we have $N = 2^{q_m}$ for the reconstruction function, and $N = 2^{q_m} - 1$ for the threshold set. For a preset maximum number of iterations I_{\max} , we define the discrepancy of two LUTs as

$$d(\mathbf{y}^{(t)}, \mathbf{y}^{(t')}) = \sqrt{\sum_{n=1}^N (y_n^{(t)} - y_n^{(t')})^2}, \quad (10)$$

where $1 \leq t < t' \leq I_{\max}$. A smaller value of the discrepancy means the two LUTs have corresponding entries similar to each other, and vice versa. For the LUTs associated to the I_{\max} decoding iterations, we first divide them into M groups. Define \mathcal{I}_m as the set of iteration indices associated to the LUTs in the m -th ($m = 1, 2, \dots, M$) group. For all LUTs with $t \in \mathcal{I}_m$, we define a merge function

$$f(\{\mathbf{y}^{(t)} : t \in \mathcal{I}_m\}) = \left[\frac{1}{|\mathcal{I}_m|} \sum_{t \in \mathcal{I}_m} \mathbf{y}^{(t)} \right], \quad (11)$$

which computes the optimized LUT by averaging the vectors $\mathbf{y}^{(t)}$, $\forall t \in \mathcal{I}_m$. We denote the obtained LUT by $\tilde{\mathbf{y}}$ and reuse it for any iteration $t \in \mathcal{I}_m$. Note that $\lceil \mathbf{x} \rceil$ returns the closest integer to each element of the vector \mathbf{x} . We denote the LUT optimized for the m -th group by $\tilde{\mathbf{y}}^{(m)}$, which is reused for all iterations $t \in \mathcal{I}_m$. To arrange the LUTs in the m -th group, we conduct greedy search by consecutive iterations based on a discrepancy threshold denoted by Δd^* . In this letter, Δd^* is determined by performing exhaustive search among $I_{\max} - 1$ discrepancy values. We denote the discrepancy value for the k -th search by $\Delta d^{(k)} = d(\mathbf{y}^{(k)}, \mathbf{y}^{(k+1)})$ for $k = 1, 2, \dots, I_{\max} - 1$. More specifically, we first consider $\Delta d^{(k)}$ as the discrepancy threshold to update $\tilde{\mathbf{y}}^{(m)}$ for the m -th group. After that, we run the modified MIM-DE with $\tilde{\mathbf{y}}^{(m)}$ and compute the mutual

information between the coded bit and the V2C message at I_{\max} denoted by $Q^{(k)}$. Given the target mutual information value Q^* , the optimal discrepancy threshold is selected as the maximum discrepancy value to achieve $Q^{(k)} \geq Q^*$, where Q^* is set to a value approaching 1. The optimization process is summarized in **Algorithm 1**.

C. Remarks

Different from [9]–[14], the joint degree distribution considered by the modified MIM-DE is not specific for a target LDPC code. This causes the performance degradation for the rate-compatible MIM-QMS decoders compared to their rate-specific counterparts. However, the performance loss can be reduced by carefully selecting the target LDPC codes in the LUT design. We quantify σ_d equivalently by the corresponding design signal-to-noise ratio (SNR) $\tau \triangleq -20\log_{10}(\sqrt{2R_c} \cdot \sigma_d^2)$, where R_c is the code rate of the LDPC code. According to extensive simulation results, the difference of τ between any two target LDPC codes is limited up to 1.2 dB in this letter for a desirable performance. It is an open problem that whether there exists a systematic way to select the target LDPC codes for acceptable deterioration in performance.

IV. SIMULATION RESULTS

In this section, we evaluate the frame error rate (FER) performance of the proposed rate-compatible MIM-QMS decoder via Monte-Carlo simulations. We also investigate the decoding latency aspects and evaluate the memory requirement of the rate-compatible MIM-QMS decoders.

TABLE I: Degree Distributions and Noise Standard Deviation σ_d for the MIM-QMS Decoders

R_c	Degree distributions $(\rho(x), \theta(x))$	Rate-specific	Rate-compatible
2/3	$\rho(x) = x^{10}$ $\theta(x) = 0.1591x + 0.4091x^2 + 0.1591x^6 + 0.2727x^7$	0.7016	0.6195
3/4	$\rho(x) = 0.3182x^{13} + 0.6818x^{14}$ $\theta(x) = 0.1136x + 0.4091x^2 + 0.4773x^5$	0.6266	
5/6	$\rho(x) = 0.7412x^{20} + 0.2588x^{21}$ $\theta(x) = 0.0706x + 0.1765x^2 + 0.7529x^3$	0.5494	

A. FER Performance

Assume that binary LDPC codewords are modulated by binary phase-shift keying (BPSK) and transmitted over the AWGNC. We denote the floating-point precision by “ ∞ ”. For comparison, we include the FER performance of the (4, 8) rate-specific MIM-QMS decoders [14], the 4-bit rate-compatible LUT-based decoder in [11], the 4-bit normalized min-sum (NMS) decoder [6], and the BP(∞) decoder. Note that the LUT-based decoder is designed based on the MIM quantization by using the dynamic programming [16]¹, and the scaling factor of the NMS decoder is optimized as 0.75. The degree distributions of the simulated LDPC codes and the design noise standard deviation σ_d for the associated MIM-QMS decoders are given in TABLE I. We set $I_{\max} = 30$ for all decoders.

Fig. 3 depicts the FER performance of the length-1296 IEEE 802.11n LDPC codes [18] with code rates $R_c = 2/3, 3/4$, and $5/6$, respectively. We can see that our proposed rate-compatible MIM-QMS decoders achieve almost the same FER performance compared to the rate-specific MIM-QMS decoders

¹Here we consider the dynamic programming instead of the information bottleneck method in [11] to realize the MIM quantization because the dynamic programming is proved to be optimal to maximize the mutual information [16]

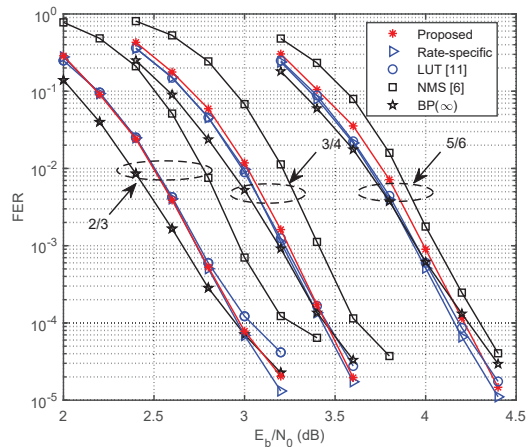


Fig. 3: FER performance of the length-1296 IEEE 802.11n LDPC codes [18] with $R_c = 2/3, 3/4$, and $5/6$.

for each code rate. Note that the performance gap between the rate-compatible MIM-QMS decoder and its rate-specific counterparts becomes larger with the increase of the code rates. This is because the rate-compatible MIM-QMS decoder is designed based on the joint degree distributions with respect to all target LDPC codes, which considers a larger portion of the VNs with low degrees for higher code rates compared to the rate-specific design. These low-degree VNs yield a slower convergence speed. Therefore, the mismatched VN degree distribution between the decoding and the LUT design leads to slightly more degradation in performance for higher code rates. Moreover, the rate-compatible MIM-QMS decoder achieves the FER performance close to the LUT-based decoder [11], and even outperforms the LUT-based decoder by about 0.1 dB in the high SNR region for $R_c = 2/3$. In addition, the rate-compatible MIM-QMS decoder surpasses the NMS decoder by up to 0.3 dB, and approaches the performance of the BP(∞) decoder within 0.15 dB for all code rates. Note that the BP(∞) decoder shows worse FER performance than the rate-compatible MIM-QMS decoders in the high SNR region. This is due to the existing of the degree-2 VNs in the code graph of the IEEE 802.11n LDPC codes. The cycles confined among these degree-2 VNs become low-weight codewords, which are the most detrimental objects for floating-point decoders [19].

B. Decoding Latency Analysis

To evaluate the decoding latency of the proposed rate-compatible MIM-QMS decoder, we first compare the convergence speed of different decoders in Section IV-A. Denote the average number of iterations required for decoding one codeword by I_{avg} . TABLE II compares I_{avg} with respect to E_b/N_0 . We can see that the rate-compatible MIM-QMS decoder requires the least I_{avg} for most of the simulated SNRs for each code rate.

We also investigate the decoding time of the proposed rate-compatible MIM-QMS decoder at each iteration. Due to the MS operation adopted for all decoders in Section IV-A, the decoding time is of $O(\lceil \log_2(d_{c,\max}) \rceil)$ for the CN update per iteration. For the VN update of the NMS decoder [6], the decoding time is of $O(\lceil \log_2(d_{v,\max}) \rceil)$ for additions while the rate-compatible LUT-based decoder [11] needs $O(d_{v,\max})$ time for table lookup operations due to the concatenating structure of LUTs. Compared to the LUT-based decoder, the rate-compatible MIM-QMS decoder adopts integer additions with $O(\lceil \log_2(d_{v,\max}) \rceil)$, and processes the table lookup operations for the threshold set and reconstruction functions in parallel.

TABLE II: Comparison of I_{avg} for Different LDPC Decoders

E_b/N_0 (dB)		2	2.2	2.4	2.6	2.8	3	3.2
I_{avg} ($R_c = 2/3$)	Proposed	19.2	13.99	10.61	8.36	6.94	5.96	5.24
	Rate-specific	19.25	14.33	11.23	9.15	7.78	6.79	6.02
	LUT [11]	19.42	14.96	11.62	9.3	7.68	6.69	5.86
	NMS [6]	27.1	21.88	16.03	10.87	7.93	6.33	5.34
E_b/N_0 (dB)		2.4	2.6	2.8	3	3.2	3.4	3.6
I_{avg} ($R_c = 3/4$)	Proposed	20.59	14.68	10.63	7.79	6.16	5.16	4.46
	Rate-specific	19.47	14.32	10.48	7.98	6.48	5.51	4.8
	LUT [11]	20.28	14.96	10.98	8.35	6.73	5.66	4.89
	NMS [6]	26.97	22.3	15.7	10.28	7.09	5.42	4.48
E_b/N_0 (dB)		3.2	3.4	3.6	3.8	4	4.2	4.4
I_{avg} ($R_c = 5/6$)	Proposed	16.16	10.46	7.34	5.31	4.22	3.54	3.06
	Rate-specific	15.02	9.99	7.14	5.4	4.4	3.74	3.26
	LUT [11]	15.48	10.46	7.35	5.5	4.41	3.71	3.2
	NMS [6]	20.64	14.39	9.12	5.82	4.24	3.42	2.88

This results in the decoding time of $O(\lceil \log_2(d_{v,\max}) \rceil + q_m)$ in total for the VN update per iteration. Since q_m is small in general, the rate-compatible MIM-QMS decoder only has slightly increased decoding time compared to the NMS decoder, and achieves much less decoding time with respect to the LUT-based decoder.

C. Comparison of Memory Requirement

To demonstrate the memory efficiency of the proposed rate-compatible MIM-QMS decoders, we compare the overall memory requirement of different quantized decoders in Section IV-A for the IEEE 802.11n LDPC codes [18] with $R_c = 2/3, 3/4$, and $5/6$. We consider that the decoder implementations are based on digital signal processors or software defined radios such that LUTs are stored in memories [11]. Note that we classify the memory into either for arithmetic computations or for storing the LUTs. For the CN update, all quantized decoders require memory for storing the two C2V messages obtained by the min-sum operation at each CN. For the VN update, both MIM-QMS decoders and the NMS decoder need to save the APP messages computed by additions for each VN. Moreover, all MIM-QMS decoders and the rate-compatible LUT-based decoder [11] need memory to store the LUTs. Without loss of generality, the memory requirement of one LUT is given by $N \cdot q_l$ bits, where q_l refers to the bit precision of one entry in the LUT. According to [11], the LUTs of the LUT-based decoder have $q_l = q_m$ and there are $d_{v,\max}$ and $|\tilde{D}_v|$ LUTs of size $N = 2^{2q_m}$ in total for the VN update and the bit decision at each iteration, respectively. The overall memory requirement for different 4-bit decoders with $I_{\max} = 30$ is summarized in TABLE III. We observe that the memory requirement for the proposed rate-compatible MIM-QMS decoder only increases by 8.28% compared to the NMS decoder. More importantly, the rate-compatible MIM-QMS decoder can reduce the memory demand by 45.37% and 94.92% compared to its rate-specific counterparts and the LUT-based decoder, respectively.

TABLE III: The Overall Memory Requirement for Different 4-bit Decoders with $I_{\max} = 30$

Decoders	Arithmetic		LUTs			Total
	CN	VN	$R_c = 2/3$	$R_c = 3/4$	$R_c = 5/6$	
Proposed	0.42 kB	1.27 kB	0.14 kB			1.83 kB
Rate-specific			0.48 kB	0.59 kB	0.59 kB	3.35 kB
NMS [6]			-			1.69 kB
LUT-based [11]			-	35.63 kB		

V. CONCLUSION

In this paper, we proposed a two-stage design approach to construct the rate-compatible MIM-QMS decoder, which significantly reduces the memory requirement for decoding. More specifically, the proposed design method first adopts the modified MIM-DE to construct the LUTs used for different code rates. The constructed LUTs are further optimized based on a merge function and their discrepancy values for two adjacent iterations. We show that the proposed rate-compatible MIM-QMS decoder reduces the memory requirement for decoding by up to 94.92% compared to the rate-compatible LUT-based decoder with faster convergence speed in the moderate-to-high SNR region. In addition, there is only minor performance loss compared to both the rate-specific MIM-QMS decoders and the floating-pointing BP decoder.

REFERENCES

- [1] R. G. Gallager, "Low-density parity-check codes," *IRE Trans. Inf. Theory*, vol. 8, no. 1, pp. 21–28, Jan. 1962.
- [2] D. Divsalar, S. Dolinar, C. R. Jones, and K. Andrews, "Capacity-approaching protograph codes," *IEEE J. Select. Areas Commun.*, vol. 27, no. 6, pp. 876–888, Aug. 2009.
- [3] T. V. Nguyen, A. Nosratinia, and D. Divsalar, "The design of rate-compatible protograph LDPC codes," *IEEE Trans. Commun.*, vol. 60, no. 10, pp. 2841–2850, Oct. 2012.
- [4] P. Chen, K. Cai, and S. Zheng, "Rate-adaptive protograph LDPC codes for multi-level-cell NAND flash memory," *IEEE Commun. Lett.*, vol. 22, no. 6, pp. 1112–1115, Jun. 2018.
- [5] T. J. Richardson, M. A. Shokrollahi, and R. L. Urbanke, "Design of capacity-approaching irregular low-density parity-check codes," *IEEE Trans. Inf. Theory*, vol. 47, no. 2, pp. 619–637, Feb. 2001.
- [6] J. Chen, A. Dholakia, E. Eleftheriou, M. P. C. Fossorier, and Xiao-Yu Hu, "Reduced-complexity decoding of LDPC codes," *IEEE Trans. Commun.*, vol. 53, no. 8, pp. 1288–1299, Aug. 2005.
- [7] P. Kang, Y. Xie, L. Yang, and J. Yuan, "Enhanced quasi-maximum likelihood decoding based on 2D modified min-sum algorithm for 5G LDPC codes," *IEEE Trans. Commun.*, vol. 68, no. 11, pp. 6669–6682, Nov. 2020.
- [8] T. T. Nguyen-Ly, V. Savin, K. Le, D. Declercq, F. Ghaffari, and O. Buncalo, "Analysis and design of cost-effective, high-throughput LDPC decoders," *IEEE Trans. Very Large Scale Integr. (VLSI) Syst.*, vol. 26, no. 3, pp. 508–521, Mar. 2018.
- [9] F. J. C. Romero and B. M. Kurkoski, "LDPC decoding mappings that maximize mutual information," *IEEE J. Select. Areas Commun.*, vol. 34, no. 9, pp. 2391–2401, Sep. 2016.
- [10] M. Meidlinger, G. Matz, and A. Burg, "Design and decoding of irregular LDPC codes based on discrete message passing," *IEEE Trans. Commun.*, vol. 68, no. 3, pp. 1329–1343, Mar. 2020.
- [11] M. Stark, L. Wang, G. Bauch, and R. D. Wesel, "Decoding rate-compatible 5G-LDPC codes with coarse quantization using the information bottleneck method," *IEEE Open J. Commun. Soc.*, vol. 1, pp. 646–660, May. 2020.
- [12] L. Wang, R. D. Wesel, M. Stark, and G. Bauch, "A reconstruction-computation-quantization (RCQ) approach to node operations in LDPC decoding," in *Proc. IEEE Global Commun. Conf.*, Dec. 2020, pp. 1–6.
- [13] X. He, K. Cai, and Z. Mei, "Mutual information-maximizing quantized belief propagation decoding of regular LDPC codes," *arXiv*, Jul. 2020. [Online]. Available: <https://arxiv.org/abs/1904.06666>
- [14] P. Kang, K. Cai, X. He, and J. Yuan, "Generalized mutual information-maximizing quantized decoding of LDPC codes with layered scheduling," *arXiv*, Jun. 2021. [Online]. Available: <https://arxiv.org/abs/2011.13147>
- [15] Z. Mei, K. Cai, and B. Dai, "Polar codes for spin-torque transfer magnetic random access memory," *IEEE Trans. on Magn.*, vol. 54, no. 11, pp. 1–5, Nov. 2018.
- [16] X. He, K. Cai, W. Song, and Z. Mei, "Dynamic programming for sequential deterministic quantization of discrete memoryless channels," *IEEE Trans. Commun.*, vol. 69, no. 6, pp. 3638–3651, Jun. 2021.
- [17] R. Tanner, "A recursive approach to low complexity codes," *IEEE Trans. Inf. Theory*, vol. 27, no. 5, pp. 533–547, Sep. 1981.
- [18] *IEEE Standard for Information Technology—Telecommunications and Information Exchange Between Systems—Local and Metropolitan Area Networks—Specific Requirements— Part 11: Wireless LAN Medium Access Control (MAC) and Physical Layer (PHY) Specifications*, IEEE Std. 802.11n, Oct. 2009.
- [19] T. Richardson, "Error floor of LDPC codes," in *Proc. 41st Annu. Allerton Conf. Commun., Control, Comput.*, Monticello, IL, Oct. 2003, pp. 1426–1435.

APPENDIX

A. The 4-bit MIM-QMS decoder for rate-2/3 802.11n LDPC code

TABLE IV: Reconstruction Functions ϕ_v and ϕ_{ch}

Iteration	$\phi_v(s), s \in \mathcal{S}$															
	0	1	2	3	4	5	6	7	8	9	10	11	12	13	14	15
1	9	7	5	3	2	1	1	0	0	-1	-1	-2	-3	-5	-7	-9
2	9	7	5	3	2	2	1	0	0	-1	-2	-2	-3	-5	-7	-9
3	9	7	5	4	2	1	1	0	0	-1	-1	-2	-4	-5	-7	-9
4	10	8	6	4	3	2	1	0	0	-1	-2	-3	-4	-6	-8	-10
5	10	7	5	4	2	1	1	0	0	-1	-1	-2	-4	-5	-7	-10
6	11	8	6	4	3	1	1	0	0	-1	-1	-3	-4	-6	-8	-11
7	13	9	7	5	3	2	1	0	0	-1	-2	-3	-5	-7	-9	-13
8	12	8	6	4	3	2	1	0	0	-1	-2	-3	-4	-6	-8	-12
9	12	9	7	5	3	2	1	0	0	-1	-2	-3	-5	-7	-9	-12
10	13	9	7	5	4	2	1	0	0	-1	-2	-4	-5	-7	-9	-13
11	13	10	7	5	3	2	1	0	0	-1	-2	-3	-5	-7	-10	-13
12	14	10	8	6	4	3	2	0	0	-2	-3	-4	-6	-8	-10	-14
13	13	9	7	5	4	2	1	0	0	-1	-2	-4	-5	-7	-9	-13
14	14	10	7	5	4	2	1	0	0	-1	-2	-4	-5	-7	-10	-14
15	14	10	7	5	3	2	1	0	0	-1	-2	-3	-5	-7	-10	-14
16	14	10	7	5	3	2	1	0	0	-1	-2	-3	-5	-7	-10	-14
17	14	10	7	5	3	2	1	0	0	-1	-2	-3	-5	-7	-10	-14
18	14	10	8	6	4	2	1	0	0	-1	-2	-4	-6	-8	-10	-14
19	14	10	8	6	4	3	2	0	0	-2	-3	-4	-6	-8	-10	-14
20	14	10	7	5	3	2	1	0	0	-1	-2	-3	-5	-7	-10	-14
21	14	10	7	5	4	2	1	0	0	-1	-2	-4	-5	-7	-10	-14
22	14	10	7	5	4	2	1	0	0	-1	-2	-4	-5	-7	-10	-14
23	14	10	7	5	3	2	1	0	0	-1	-2	-3	-5	-7	-10	-14
24	14	10	7	5	4	2	1	0	0	-1	-2	-4	-5	-7	-10	-14
25	14	10	7	5	3	2	1	0	0	-1	-2	-3	-5	-7	-10	-14
26	14	10	7	5	3	2	1	0	0	-1	-2	-3	-5	-7	-10	-14
27	14	10	7	5	3	2	1	0	0	-1	-2	-3	-5	-7	-10	-14
28	14	10	7	5	3	2	1	0	0	-1	-2	-3	-5	-7	-10	-14
29	14	10	7	5	3	2	1	1	-1	-1	-2	-3	-5	-7	-10	-14
30	14	10	7	5	4	2	1	1	-1	-1	-2	-4	-5	-7	-10	-14

Iteration	$\phi_{ch}(l), l \in \mathcal{L}$															
	0	1	2	3	4	5	6	7	8	9	10	11	12	13	14	15
1-11	14	10	7	6	4	3	2	1	-1	-2	-3	-4	-6	-7	-10	-14
12	13	9	7	5	4	3	2	1	-1	-2	-3	-4	-5	-7	-9	-13
13	14	10	7	6	4	3	2	1	-1	-2	-3	-4	-6	-7	-10	-14
14	14	10	7	6	4	3	2	1	-1	-2	-3	-4	-6	-7	-10	-14
15	13	9	7	5	4	3	2	1	-1	-2	-3	-4	-5	-7	-9	-13
16	13	9	7	5	4	3	2	1	-1	-2	-3	-4	-5	-7	-9	-13
17	12	8	6	5	4	2	1	0	0	-1	-2	-4	-5	-6	-8	-12
18	12	9	6	5	4	2	1	0	0	-1	-2	-4	-5	-6	-9	-12
19	12	8	6	5	4	2	1	0	0	-1	-2	-4	-5	-6	-8	-12
20	11	8	6	4	3	2	1	0	0	-1	-2	-3	-4	-6	-8	-11
21	11	8	6	4	3	2	1	0	0	-1	-2	-3	-4	-6	-8	-11
22	11	8	6	5	3	2	1	0	0	-1	-2	-3	-5	-6	-8	-11
23	10	7	5	4	3	2	1	0	0	-1	-2	-3	-4	-5	-7	-10
24	10	7	5	4	3	2	1	0	0	-1	-2	-3	-4	-5	-7	-10
25	9	7	5	4	3	2	1	0	0	-1	-2	-3	-4	-5	-7	-9
26	9	6	5	4	3	2	1	0	0	-1	-2	-3	-4	-5	-6	-9
27	9	6	5	4	3	2	1	0	0	-1	-2	-3	-4	-5	-6	-9
28	8	6	4	3	2	2	1	0	0	-1	-2	-2	-3	-4	-6	-8
29	8	5	4	3	2	2	1	0	0	-1	-2	-2	-3	-4	-5	-8
30	7	5	4	3	2	1	1	0	0	-1	-1	-2	-3	-4	-5	-7

TABLE V: Threshold sets Γ_v , Γ_{ch} , and Γ_e

Iteration	Γ_v														
	γ_1	γ_2	γ_3	γ_4	γ_5	γ_6	γ_7	γ_8	γ_9	γ_{10}	γ_{11}	γ_{12}	γ_{13}	γ_{14}	γ_{15}
1	12	9	7	5	4	3	2	1	-1	-2	-3	-4	-6	-8	-11
2	12	9	7	5	4	3	2	1	0	-1	-3	-4	-6	-8	-11
3	13	10	8	6	4	3	2	0	-1	-2	-3	-5	-7	-9	-12
4	13	9	7	5	4	3	2	1	0	-1	-2	-4	-6	-8	-12
5	13	10	8	6	4	3	2	1	0	-1	-2	-4	-6	-8	-12
6	15	11	8	6	4	3	2	0	-1	-2	-3	-5	-7	-10	-14
7	14	10	7	5	4	2	1	0	-1	-2	-3	-4	-6	-9	-13
8	16	12	9	7	5	3	2	1	0	-1	-2	-4	-6	-9	-13
9	16	12	9	7	5	4	2	1	0	-1	-3	-4	-6	-9	-13
10	15	11	8	6	4	3	2	0	-1	-2	-3	-5	-7	-10	-14
11	16	12	9	7	5	4	2	1	-1	-3	-4	-6	-8	-11	-15
12	15	11	9	7	5	3	2	1	0	-1	-2	-4	-6	-8	-12
13	15	11	8	6	4	3	2	0	-1	-2	-3	-5	-7	-10	-14
14	16	11	8	6	4	3	2	0	-1	-2	-3	-5	-7	-10	-15
15	14	10	7	5	4	3	2	1	0	-1	-2	-4	-6	-9	-13
16	16	11	8	6	4	2	1	0	-1	-2	-3	-5	-7	-10	-15
17	15	11	8	6	4	3	2	1	0	-1	-2	-4	-6	-8	-12
18	16	12	9	7	5	4	2	1	0	-1	-3	-4	-6	-9	-13
19	16	11	8	5	3	2	1	0	-1	-2	-3	-5	-7	-10	-15
20	13	9	6	4	3	2	1	0	-1	-2	-3	-5	-7	-9	-13
21	13	9	7	5	3	2	1	0	-1	-2	-3	-4	-6	-8	-12
22	15	10	7	5	3	2	1	0	-1	-2	-3	-5	-7	-10	-15
23	13	9	7	5	4	3	2	1	0	-1	-2	-4	-6	-8	-12
24	14	10	7	5	4	3	2	1	0	-1	-2	-4	-6	-9	-13
25	13	9	7	5	3	2	1	0	-1	-2	-3	-4	-6	-8	-12
26	13	9	7	5	3	2	1	0	-1	-2	-3	-4	-6	-8	-12
27	13	9	7	5	4	3	2	1	0	-1	-2	-4	-6	-8	-12
28	13	9	6	4	3	2	1	0	-1	-2	-3	-4	-6	-8	-12
29	14	10	8	6	4	3	2	1	0	-1	-2	-3	-5	-8	-12
30	12	8	6	5	4	3	2	1	0	-1	-2	-3	-5	-7	-11

Γ_{ch} (in LLR format)														
γ_1	γ_2	γ_3	γ_4	γ_5	γ_6	γ_7	γ_8	γ_9	γ_{10}	γ_{11}	γ_{12}	γ_{13}	γ_{14}	γ_{15}
5.50	4.04	3.06	2.30	1.64	1.06	0.52	0	-0.52	-1.06	-1.64	-2.30	-3.06	-4.04	-5.50

Iteration	Γ_e
	γ_1
1-5	0
6	1
7	0
8-28	1
29	0
30	1

B. The 4-bit MIM-QMS decoder for rate-3/4 802.11n LDPC code

TABLE VI: Reconstruction Functions ϕ_v and ϕ_{ch}

Iteration	$\phi_v(s), s \in \mathcal{S}$															
	0	1	2	3	4	5	6	7	8	9	10	11	12	13	14	15
1	12	8	6	4	3	2	1	0	0	-1	-2	-3	-4	-6	-8	-12
2	12	9	7	5	3	2	1	0	0	-1	-2	-3	-5	-7	-9	-12
3	13	10	7	5	3	2	1	0	0	-1	-2	-3	-5	-7	-10	-13
4-6	13	10	7	5	4	2	1	0	0	-1	-2	-4	-5	-7	-10	-13
7	13	10	7	6	4	2	1	0	0	-1	-2	-4	-6	-7	-10	-13
8	14	10	7	6	4	2	1	0	0	-1	-2	-4	-6	-7	-10	-14
9	14	10	8	6	4	2	1	0	0	-1	-2	-4	-6	-8	-10	-14
10	15	11	8	6	5	3	2	1	-1	-2	-3	-5	-6	-8	-11	-15
11	15	11	8	6	5	3	2	0	0	-2	-3	-5	-6	-8	-11	-15
12	14	10	8	6	4	3	2	0	0	-2	-3	-4	-6	-8	-10	-14
13	14	10	8	6	4	2	1	0	0	-1	-2	-4	-6	-8	-10	-14
14	15	11	9	7	5	3	2	1	-1	-2	-3	-5	-7	-9	-11	-15
15	15	11	9	7	5	3	2	0	0	-2	-3	-5	-7	-9	-11	-15
16	15	11	8	6	4	3	1	0	0	-1	-3	-4	-6	-8	-11	-15
17	15	11	8	6	4	3	1	0	0	-1	-3	-4	-6	-8	-11	-15
18	15	11	8	6	4	3	2	0	0	-2	-3	-4	-6	-8	-11	-15
19	16	11	8	6	5	3	2	0	0	-2	-3	-5	-6	-8	-11	-16
20	18	14	10	8	6	4	2	0	0	-2	-4	-6	-8	-10	-14	-18
21	18	13	10	7	5	4	2	1	-1	-2	-4	-5	-7	-10	-13	-18
22	18	13	10	8	6	4	2	1	-1	-2	-4	-6	-8	-10	-13	-18
23	18	13	10	8	6	4	2	1	-1	-2	-4	-6	-8	-10	-13	-18
24	18	13	10	8	5	4	2	1	-1	-2	-4	-5	-8	-10	-13	-18
25	18	13	10	8	6	4	2	0	0	-2	-4	-6	-8	-10	-13	-18
26	18	13	9	7	5	4	2	0	0	-2	-4	-5	-7	-9	-13	-18
27	18	13	9	7	5	3	2	0	0	-2	-3	-5	-7	-9	-13	-18
28	18	12	8	6	4	3	2	1	-1	-2	-3	-4	-6	-8	-12	-18
29	18	12	8	6	4	3	1	0	0	-1	-3	-4	-6	-8	-12	-18
30	18	12	8	6	4	3	2	0	0	-2	-3	-4	-6	-8	-12	-18

Iteration	$\phi_{ch}(l), l \in \mathcal{L}$															
	0	1	2	3	4	5	6	7	8	9	10	11	12	13	14	15
1-20	18	12	9	7	5	4	2	1	-1	-2	-4	-5	-7	-9	-12	-18
21	17	12	9	7	5	3	2	1	-1	-2	-3	-5	-7	-9	-12	-17
22	16	11	8	6	5	3	2	1	-1	-2	-3	-5	-6	-8	-11	-16
23	16	11	9	6	5	3	2	1	-1	-2	-3	-5	-6	-9	-11	-16
24	15	10	8	6	4	3	2	1	-1	-2	-3	-4	-6	-8	-10	-15
25	15	10	8	6	4	3	2	1	-1	-2	-3	-4	-6	-8	-10	-15
26	13	9	7	5	4	3	2	1	-1	-2	-3	-4	-5	-7	-9	-13
27	12	8	6	5	4	2	1	0	0	-1	-2	-4	-5	-6	-8	-12
28	12	8	6	5	3	2	1	0	0	-1	-2	-3	-5	-6	-8	-12
29	11	8	6	4	3	2	1	0	0	-1	-2	-3	-4	-6	-8	-11
30	10	7	5	4	3	2	1	0	0	-1	-2	-3	-4	-5	-7	-10

TABLE VII: Threshold sets Γ_v , Γ_{ch} , and Γ_e

Iteration	Γ_v														
	γ_1	γ_2	γ_3	γ_4	γ_5	γ_6	γ_7	γ_8	γ_9	γ_{10}	γ_{11}	γ_{12}	γ_{13}	γ_{14}	γ_{15}
1	15	11	9	7	5	3	2	0	-1	-2	-4	-6	-8	-10	-14
2	16	12	9	7	5	3	2	0	-1	-2	-4	-6	-8	-11	-15
3	16	12	9	7	5	3	2	1	-1	-2	-4	-6	-8	-11	-15
4	16	12	9	7	5	3	1	0	-1	-2	-4	-6	-8	-11	-15
5	16	12	9	7	5	3	2	1	0	-2	-4	-6	-8	-11	-15
6	16	12	9	7	5	3	2	1	0	-2	-4	-6	-8	-11	-15
7	17	12	9	7	5	3	2	1	0	-2	-4	-6	-8	-11	-16
8	17	12	9	7	5	3	2	1	0	-2	-4	-6	-8	-11	-16
9	17	12	9	7	5	3	1	0	-2	-4	-6	-8	-10	-13	-18
10	18	13	10	8	6	4	2	1	-1	-3	-5	-7	-9	-12	-17
11	17	12	9	7	5	4	2	1	-1	-3	-4	-6	-8	-11	-16
12	17	12	9	7	5	3	2	0	-1	-2	-4	-6	-8	-11	-16
13	17	12	9	7	5	3	1	0	-2	-4	-6	-8	-10	-13	-18
14	18	13	10	8	6	4	2	0	-1	-3	-5	-7	-9	-12	-17
15-18	17	12	9	7	5	3	2	0	-1	-2	-4	-6	-8	-11	-16
19	20	15	11	8	6	4	2	1	-1	-3	-5	-7	-10	-14	-19
20	20	14	10	7	5	3	1	0	-2	-4	-6	-8	-10	-13	-19
21	20	14	10	8	6	4	2	0	-2	-4	-6	-8	-11	-14	-20
22	18	13	10	8	6	4	2	0	-1	-3	-5	-7	-9	-12	-17
23	20	14	11	8	6	4	2	0	-1	-3	-5	-7	-10	-13	-19
24	17	12	9	7	5	3	1	0	-1	-3	-5	-7	-10	-13	-18
25	19	13	10	8	6	4	2	1	-1	-3	-5	-7	-9	-12	-18
26	18	12	9	7	5	3	2	1	0	-2	-4	-6	-8	-11	-17
27	17	11	8	6	4	3	2	1	-1	-2	-3	-5	-7	-10	-16
28	18	12	9	7	5	3	2	1	0	-1	-2	-4	-6	-9	-15
29	16	11	8	6	4	3	1	0	-1	-2	-3	-5	-7	-10	-15
30	16	11	8	6	4	3	2	1	0	-1	-2	-4	-6	-9	-14

Γ_{ch} (in LLR format)														
γ_1	γ_2	γ_3	γ_4	γ_5	γ_6	γ_7	γ_8	γ_9	γ_{10}	γ_{11}	γ_{12}	γ_{13}	γ_{14}	γ_{15}
6.02	4.38	3.32	2.48	1.78	1.14	0.56	0	-0.56	-1.14	-1.78	-2.48	-3.32	-4.38	-6.02

Iteration	Γ_e
	γ_1
1-11	1
12	0
13	1
14	0
15	1
16	1
17-28	0
29	1
30	1

C. The 4-bit MIM-QMS decoder for rate-5/6 802.11n LDPC code

TABLE VIII: Reconstruction Functions ϕ_v and ϕ_{ch}

Iteration	$\phi_v(s), s \in \mathcal{S}$															
	0	1	2	3	4	5	6	7	8	9	10	11	12	13	14	15
1	16	11	8	6	4	2	1	0	0	-1	-2	-4	-6	-8	-11	-16
2	16	11	9	6	4	3	1	0	0	-1	-3	-4	-6	-9	-11	-16
3-6	17	12	9	7	5	3	2	0	0	-2	-3	-5	-7	-9	-12	-17
7	17	13	10	7	5	3	2	0	0	-2	-3	-5	-7	-10	-13	-17
8	18	13	10	7	5	3	2	0	0	-2	-3	-5	-7	-10	-13	-18
9	18	13	10	7	5	3	1	0	0	-1	-3	-5	-7	-10	-13	-18
10-13	18	13	10	7	5	3	2	1	-1	-2	-3	-5	-7	-10	-13	-18
14	18	14	11	8	5	3	2	1	-1	-2	-3	-5	-8	-11	-14	-18
15	18	14	10	8	5	3	2	1	-1	-2	-3	-5	-8	-10	-14	-18
16	19	14	11	8	6	4	2	1	-1	-2	-4	-6	-8	-11	-14	-19
17	19	14	11	8	5	4	2	1	-1	-2	-4	-5	-8	-11	-14	-19
18	18	14	10	8	5	4	2	1	-1	-2	-4	-5	-8	-10	-14	-18
19	19	14	10	8	5	4	2	1	-1	-2	-4	-5	-8	-10	-14	-19
20	20	14	11	8	6	4	2	1	-1	-2	-4	-6	-8	-11	-14	-20
21	20	15	11	8	6	4	2	1	-1	-2	-4	-6	-8	-11	-15	-20
22	21	15	11	8	6	4	2	1	-1	-2	-4	-6	-8	-11	-15	-21
23	21	16	12	9	7	4	3	1	-1	-3	-4	-7	-9	-12	-16	-21
24	22	17	12	9	7	4	2	1	-1	-2	-4	-7	-9	-12	-17	-22
25	23	17	13	10	7	4	3	1	-1	-3	-4	-7	-10	-13	-17	-23
26	25	19	14	10	7	5	3	1	-1	-3	-5	-7	-10	-14	-19	-25
27	25	19	14	11	8	5	3	1	-1	-3	-5	-8	-11	-14	-19	-25
28	25	19	14	10	8	5	3	1	-1	-3	-5	-8	-10	-14	-19	-25
29	25	18	12	8	6	4	2	1	-1	-2	-4	-6	-8	-12	-18	-25
30	25	17	13	10	7	5	3	1	-1	-3	-5	-7	-10	-13	-17	-25

Iteration	$\phi_{ch}(l), l \in \mathcal{L}$															
	0	1	2	3	4	5	6	7	8	9	10	11	12	13	14	15
1-25	25	17	13	10	7	5	3	1	-1	-3	-5	-7	-10	-13	-17	-25
26	25	17	13	9	7	5	3	1	-1	-3	-5	-7	-9	-13	-17	-25
27	23	16	12	9	6	4	3	1	-1	-3	-4	-6	-9	-12	-16	-23
28	20	14	10	8	6	4	2	1	-1	-2	-4	-6	-8	-10	-14	-20
29	18	12	9	7	5	3	2	1	-1	-2	-3	-5	-7	-9	-12	-18
30	16	11	8	6	4	3	2	1	-1	-2	-3	-4	-6	-8	-11	-16

TABLE IX: Threshold sets Γ_v , Γ_{ch} , and Γ_e

Iteration	Γ_v														
	γ_1	γ_2	γ_3	γ_4	γ_5	γ_6	γ_7	γ_8	γ_9	γ_{10}	γ_{11}	γ_{12}	γ_{13}	γ_{14}	γ_{15}
1	20	15	12	9	6	4	2	0	-2	-4	-6	-8	-11	-14	-19
2	22	17	13	10	7	5	3	1	-1	-3	-5	-7	-10	-14	-20
3	21	15	11	8	6	4	2	0	-2	-4	-6	-9	-12	-16	-21
4	23	17	13	10	7	5	3	1	-1	-3	-5	-7	-10	-14	-20
5	21	15	11	8	6	4	2	0	-2	-4	-6	-9	-12	-16	-22
6	23	17	13	10	7	5	3	1	-1	-3	-5	-7	-10	-14	-20
7	22	16	12	9	6	4	2	0	-2	-4	-6	-9	-12	-16	-22
8	22	16	12	9	6	4	2	1	-1	-3	-5	-8	-11	-15	-21
9	23	17	13	10	7	5	3	1	-1	-3	-5	-7	-10	-14	-20
10	22	16	12	9	6	4	2	0	-2	-4	-6	-8	-11	-15	-21
11	22	16	12	9	7	5	3	1	-1	-3	-5	-8	-11	-15	-21
12	22	16	12	9	6	4	2	0	-2	-4	-6	-8	-11	-15	-21
13	23	17	13	10	7	5	3	1	-1	-3	-5	-8	-11	-15	-21
14	22	16	12	9	7	5	3	1	-1	-3	-5	-8	-11	-15	-21
15	23	17	13	10	7	5	3	1	-1	-3	-5	-8	-11	-15	-21
16	23	17	13	10	7	5	3	1	-1	-3	-5	-8	-11	-15	-22
17	22	16	12	9	7	5	3	1	-1	-3	-5	-8	-11	-15	-21
18	23	16	12	9	7	5	3	1	-1	-3	-5	-8	-11	-15	-22
19	24	17	13	10	7	5	3	1	-1	-3	-5	-8	-11	-15	-22
20	24	17	13	10	7	5	3	1	-1	-3	-5	-8	-11	-15	-22
21	24	17	12	9	6	4	2	0	-2	-4	-6	-9	-12	-16	-23
22	24	17	13	10	7	5	3	1	-2	-4	-6	-9	-12	-16	-23
23	25	18	13	10	7	4	2	0	-2	-4	-6	-9	-12	-17	-24
24	25	18	13	10	7	4	2	0	-2	-4	-6	-9	-12	-17	-24
25	27	19	14	10	7	5	3	1	-1	-3	-6	-9	-13	-18	-26
26	29	21	16	12	9	6	4	2	-1	-3	-6	-9	-13	-18	-26
27	28	20	15	11	8	5	3	0	-2	-4	-7	-10	-14	-19	-27
28	25	17	12	8	6	4	2	1	-1	-3	-5	-7	-11	-16	-24
29	24	17	13	10	7	5	3	1	-1	-4	-6	-9	-12	-16	-23
30	25	17	13	10	8	5	3	1	0	-2	-4	-7	-10	-14	-22

Γ_{ch} (in LLR format)														
γ_1	γ_2	γ_3	γ_4	γ_5	γ_6	γ_7	γ_8	γ_9	γ_{10}	γ_{11}	γ_{12}	γ_{13}	γ_{14}	γ_{15}
6.64	4.80	3.60	2.68	1.90	1.24	0.60	0	-0.60	-1.24	-1.90	-2.68	-3.60	-4.80	-6.64

Iteration	Γ_e
	γ_1
1-4	0
5-7	1
8	0
9-29	1
30	0

D. The 4-bit rate-compatible MIM-QMS decoder for 802.11n LDPC codes

TABLE X: Reconstruction Functions ϕ_v and ϕ_{ch}

Iteration	$\phi_v(s), s \in \mathcal{S}$															
	0	1	2	3	4	5	6	7	8	9	10	11	12	13	14	15
1-14	11	8	6	4	3	2	1	0	0	-1	-2	-3	-4	-6	-8	-11
15	13	10	7	5	3	2	1	0	0	-1	-2	-3	-5	-7	-10	-13
16	13	10	7	5	3	2	1	0	0	-1	-2	-3	-5	-7	-10	-13
17-30	14	10	7	5	3	2	1	0	0	-1	-2	-3	-5	-7	-10	-14

Iteration	$\phi_{ch}(l), l \in \mathcal{L}$															
	0	1	2	3	4	5	6	7	8	9	10	11	12	13	14	15
1-21	14	10	7	5	4	3	2	1	-1	-2	-3	-4	-5	-7	-10	-14
22-30	10	7	5	4	3	2	1	0	0	-1	-2	-3	-4	-5	-7	-10

TABLE XI: Threshold sets Γ_v , Γ_{ch} , and Γ_e

Iteration	Γ_v														
	γ_1	γ_2	γ_3	γ_4	γ_5	γ_6	γ_7	γ_8	γ_9	γ_{10}	γ_{11}	γ_{12}	γ_{13}	γ_{14}	γ_{15}
1-3	12	9	7	5	3	2	1	0	-1	-2	-3	-4	-6	-8	-11
4-11	13	9	7	5	4	3	2	1	0	-1	-2	-4	-6	-8	-12
12	14	10	7	5	4	3	2	1	0	-1	-2	-4	-6	-9	-13
13	14	10	7	5	4	3	2	1	0	-1	-2	-4	-6	-9	-13
14-18	15	11	8	6	4	3	2	1	0	-1	-2	-4	-6	-9	-13
19	15	10	7	5	3	2	1	0	-1	-2	-3	-5	-7	-10	-14
20	15	10	7	5	3	2	1	0	-1	-2	-3	-5	-7	-10	-14
21	16	12	9	7	5	3	2	1	0	-1	-2	-4	-6	-9	-13
22	15	11	8	6	4	3	2	1	0	-1	-3	-4	-6	-9	-13
23	15	11	8	6	4	3	2	1	0	-1	-3	-4	-6	-9	-13
24-27	14	9	7	5	3	2	1	0	-1	-2	-3	-4	-6	-8	-13
28	14	10	8	6	4	3	2	1	0	-1	-2	-3	-5	-7	-11
29	14	10	8	6	4	3	2	1	0	-1	-2	-3	-5	-7	-11
30	12	8	6	5	4	3	2	1	0	-1	-2	-3	-5	-7	-11

Γ_{ch} (in LLR format)														
γ_1	γ_2	γ_3	γ_4	γ_5	γ_6	γ_7	γ_8	γ_9	γ_{10}	γ_{11}	γ_{12}	γ_{13}	γ_{14}	γ_{15}
6.06	4.42	3.34	2.50	1.78	1.16	0.56	0	-0.56	-1.16	-1.78	-2.50	-3.34	-4.42	-6.06

Iteration	Γ_e
	γ_1
1-30	1